Rapid and precise absolute distance measurements at long range

I. Coddington*, W. C. Swann, L. Nenadovic and N. R. Newbury*

The ability to determine absolute distance to an object is one of the most basic measurements of remote sensing. High-precision ranging has important applications in both large-scale manufacturing and in future tight formation-flying satellite missions, where rapid and precise measurements of absolute distance are critical for maintaining the relative pointing and position of the individual satellites. Using two coherent broadband fibre-laser frequency comb sources, we demonstrate a coherent laser ranging system that combines the advantages of time-of-flight and interferometric approaches to provide absolute distance measurements, simultaneously from multiple reflectors, and at low power. The pulse time-of-flight yields a precision of 3 μm with an ambiguity range of 1.5 m in 200 μs. Through the optical carrier phase, the precision is improved to better than 5 nm at 60 ms, and through the radio-frequency phase the ambiguity range is extended to 30 km, potentially providing 2 parts in 10^{13} ranging at long distances.

Multiple satellites flying in a precision formation can effectively act as a single distributed instrument and provide entirely new capabilities for space-based sciences. Formations would enable higher-resolution searches for extraterrestrial planets by providing a large synthetic aperture, enable direct imaging of a black hole by supporting an X-ray telescope distributed across satellites, or enable tests of general relativity through accurate measurements of satellite spacing in a gravitational field[1–11]. The formation acts as a single instrument only if the relative spacing and pointing of the satellites is tightly maintained, which is made possible by comparing distance measurements between multiple reference points on the satellites and feeding back to the satellite position and pointing.

In intrasatellite ranging, and similarly in manufacturing applications[12], there are three critical parameters: precision/accuracy, ambiguity range and update rate. High precision is particularly important in maintaining the pointing; for example, coherent combining of 1-m sub-apertures to form a synthetic aperture of 100-m diameter requires a relative pointing accuracy of less than ($\lambda/100$ m) rad for each sub-aperture, which in turn requires distance measurements at the sub-aperture edges with less than $\lambda \times$ (1 m/100 m) accuracy, or a few nanometres at optical wavelengths. The ambiguity range characterizes the measurement range window; longer distances are aliased back to within the ambiguity range. Larger ambiguity range requires less *a priori* distance knowledge. Finally, fast millisecond-scale update rates are needed for effective feedback. Many of these requirements push or exceed the capabilities of current 'stand off' ranging technology, but are achievable using an optical frequency comb, as shown here.

Generally speaking, laser ranging is the determination of the phase shift on a signal after traversing a given distance. Crudely, shorter-wavelength signals offer greater resolution, and longer-wavelength signals offer greater ambiguity range. For instance, the widely used continuous-wave (c.w.) laser interferometer measures the phase of optical wavelengths to achieve sub-nanometre resolution[13–15]. However, measurements are limited to relative range changes as the ambiguity range equals half the laser wavelength. Alternatively, laser radar (LIDAR) measures distance through pulsed or radio-frequency (rf)-modulated waveforms. (For pulsed systems,

one simply measures the time-of-flight.) These systems offer large ambiguity ranges but with ~50–100 μm resolution[12,16–18].

Multiwavelength interferometry (MWI) combines measurements at several optical wavelengths, which effectively generates a longer 'synthetic wavelength', and therefore a reasonable ambiguity range while maintaining sub-wavelength resolution[19–26]. However, these systems are vulnerable to systematic errors from spurious reflections, and extending the ambiguity range beyond a millimetre can require slow scanning. Nevertheless, with extensive care in minimizing spurious reflections, the MSTAR[27] system has successfully used MWI for sub-micrometre ranging.

Femtosecond optical frequency combs offer an intriguing solution to the intrasatellite ranging problem[28,29]. From the early work by Minoshima and colleagues[18], combs have been incorporated into precision ranging systems using the various approaches discussed above[23–26,30–33]. In particular, the comb output has been used directly in several experiments to take advantage of its coherence in both the rf and optical domains[27,33,34]. Building on this earlier work, we demonstrate here a comb-based coherent LIDAR that provides a unique combination of precision, speed and large ambiguity range.

Results

Measurement concept. In this work the pulsed nature of a comb is combined with the coherence of the carrier, allowing for a time-of-flight measurement simultaneously with an interferometric measurement based on carrier phase[30,33,34]. We implement this approach with dual coherent frequency combs and achieve a nanometre level of precision with an ambiguity range of 1.5 m in 60 ms at low light levels and with high immunity to spurious reflections. The ambiguity range is easily extended to 30 km. Finally, the time-resolved signal also permits measurements between multiple reference planes in a single beam path. This host of features is unavailable in any other single system.

Our approach follows the footprint of MSTAR as well as related spectroscopy work[35–40], in that we use of a pair of stabilized femtosecond laser frequency combs having pulse trains of slightly different repetition periods (T_r and $T_r - \Delta T_r$). In Fig. 1, we focus on the time-domain picture. One comb serves as the 'signal' source and
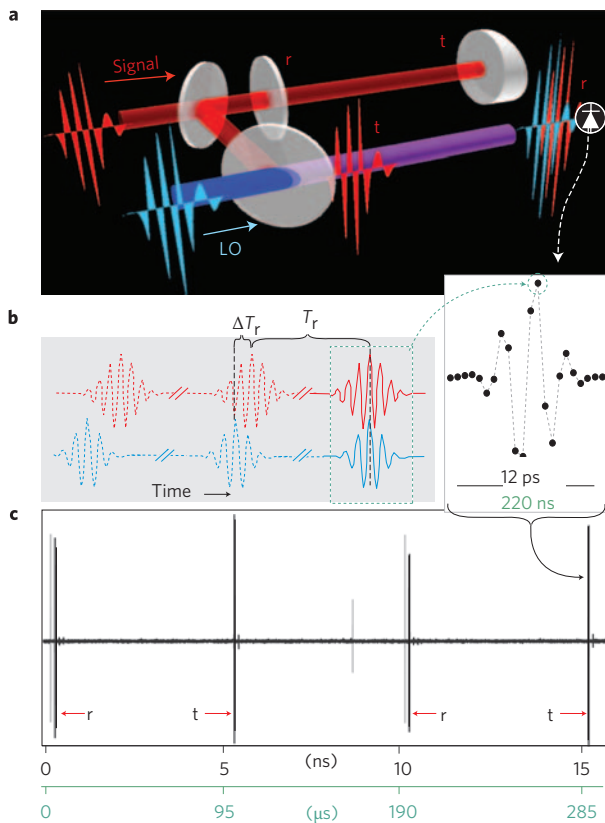
Figure 1 | Ranging concept. a, A high-repetition-rate 'signal' source transmits pulses that are reflected from two partially reflecting planes (glass plates): the reference (r) and the target (t). The reference is a flat plate and yields two reflections, the first of which is ignored. Distance is measured as the time delay between the reflections from the back surface of the reference flat and the front of the target. **b**, The signal pulses are detected through linear optical sampling against a local oscillator (LO). The LO generates pulses at a slightly different repetition rate. Every repetition period (T_r), the LO pulse 'slips' by ΔT_r relative to the signal pulses, and samples a slightly different portion of the signal. Consecutive samples of the overlap between the signal and LO yield a high-resolution measurement of the returning target and reference pulses. Actual data are shown on the right side, where each discrete point corresponds to a single digitized sample and only the immediate overlap region is shown. **c**, The measured voltage out of the detector in both real time (lower scale) and effective time (upper scale) for a target and reference plane separated by 0.76 m. A full 'scan' of the LO pulse across the signal pulse is accomplished every ~200 μs in real time and every ~10 ns in effective time. Two such scans are shown to illustrate the fast, repetitive nature of the measurement. Also seen are two peaks in grey which are spurious reflections of the launch optics.

samples a distance path defined by reflections off a target and reference plane. The second comb serves as a broadband local oscillator (LO), and recovers range information in an approach equivalent to linear optical sampling[41,42] (that is, a heterodyne cross-correlation between the signal and LO). The heterodyne detection provides shot-noise limited performance so that even weak return signals can be detected and the information in the carrier phase is retained. Similar to a down-sampling oscilloscope, measurements can be made with slow detectors and electronics (50–100 MHz) and are easily mapped back into the original femtosecond timescale. An entire scan of the signal return, shown in Fig. 1c, is completed every $T_{update} = T_r^2/\Delta T_r$. For our experiment the two frequency combs operate at repetition rates of 100.021 and 100.016 MHz, giving $T_r \approx 10$ ns, $T_{update} = 1/5{,}190$ Hz ≈ 200 μs
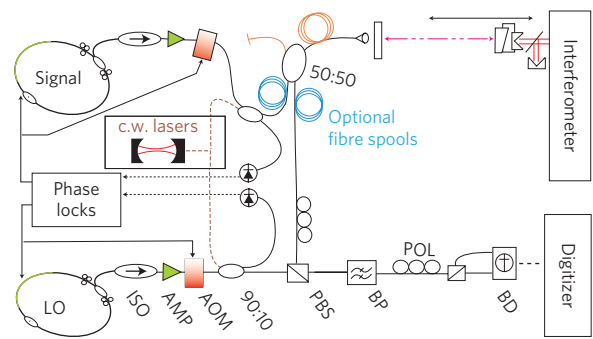
Figure 2 | Schematic of the experimental set-up. Two erbium fibre frequency combs are each phase-locked to two c.w. reference lasers at 1,535 and 1,550 nm (ref. 38). For each laser an intercavity piezo-electric transducer and external acousto-optic modulator (AOM) provide modulation for one lock, and pump current modulation is sufficient for the second. A c.w. interferometer is used to monitor the relative target position. The signal pulse trains are combined with the LO on a polarizing beamsplitter (PBS), optically filtered with a 3-nm bandpass (BP) at 1,562 nm, directed to a balanced detector (BD), and finally digitized at 14 bits synchronously with the LO. The total detected signal power per reflection is ~0.4 μW, or 4 fJ per pulse. ISO, isolator; AMP, erbium fibre amplifier; POL, polarization control; 90:10 and 50:50 are splitter ratios. Optional (1.14-km) fibre spools are included in two configurations, matched pairs (blue) and bidirectional (orange).

and $\Delta T_r \approx 0.5$ ps. A 3-nm bandpass filter limits the transmitted optical bandwidth to much less than $1/(4\Delta T_r)$ in order to meet the Nyquist condition for sampling (discussed later). Figure 2 shows a detailed schematic.

Given the digitized signal in Fig. 1c, the distance between target and reference reflections is calculated by the use of Fourier processing. Mathematically, the LO and signal electric field pulse trains are $\sum_n e^{in\theta_{LO}}E_{LO}(t - nT_r)$ and $\sum_n e^{in\theta_S}E_S(t - n(T_r - \Delta T_r))$, respectively, where $E_{LO(S)}$ is the electric field of a single pulse, n is the pulse index and $\theta_{LO(S)}$ is the carrier-envelope offset phase. For the nth pulse the detected voltage signal is proportional to the temporal overlap between the LO and delayed signal pulses, given by $V(t_{eff}) = \int E^*_{LO}(t)[E_S(t + t_{eff} - \tau_r) + e^{i\psi}E_S(t + t_{eff} - \tau_t)]dt$, where the effective time is $t_{eff} = n\Delta T_r$, ψ accounts for the π differential phase shift upon reflection as well as the relative Gouy phase, τ_r and τ_t are the delays on the reference and target pulses, respectively, and we assume for simplicity that $\theta_{LO} = \theta_S$. To find the relative delay $\tau = \tau_t - \tau_r$ between the target and reference reflection peaks in Fig. 1c, we time-window the separate contributions to $V(t_{eff})$ from the reference and target(s) to find $V^r(t_{eff})$ and $V^t(t_{eff})$. The Fourier transforms of the two are simply related by $\tilde{V}^t(\nu) = e^{i\varphi(\nu)+i\psi}\tilde{V}^r(\nu)$, with the relative spectral phase of $\varphi(\nu) = 2\pi\tau\nu$. Converting from τ to measured distance L, and including the dispersion of the air path, gives the relative spectral phase

$$\varphi(\nu) = 4\pi L/\lambda_c + (4\pi L/v_{group})(\nu - \nu_c) \qquad (1)$$

where ν_c is the carrier frequency, v_{group} is the group velocity at carrier frequency, and λ_c is the carrier wavelength, calculated at measured atmospheric conditions[43].

A simple linear fit $\varphi = \varphi_0 + b(\nu - \nu_c)$ gives the time-of-flight measurement through $L_{tof} = b(v_{group}/4\pi)$ and the high-precision interferometric distance measurement through $L_{int} = (\varphi_0 + 2\pi m)$ $(\lambda_c/4\pi)$. The $2\pi m$ ambiguity reflects the inherent $\lambda_c/2$ range ambiguity in any interferometric measurement. From equation (1) it is clear the system is identical to MWI with many simultaneously transmitted wavelengths (equal to the number of transmitted comb lines).
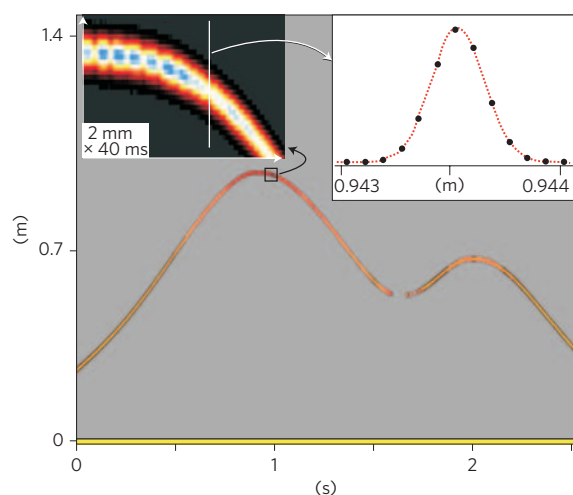
Figure 3 | Real-time image of the range versus time for a moving target (shown in false colour). Every 200 μs, the system scans the entire 1.5-m ambiguity range of the system. Sequential scans are stacked horizontally to yield an image tracking the target motion. The signal at zero distance is the reference plane, and the moving signal represents the target. The upper left inset shows an expanded view where the discrete nature of the sampling is visible. The upper right inset shows a cross-section of the return signal (magnitude squared of the detected electric field). The signal width is set by the 0.42 THz signal $1/e^2$ bandwidth.

This approach is robust to systematic shifts for several reasons. First and most importantly, the time gating eliminates shifts due to spurious reflections outside of the ±30 ps (±4.5 mm) range window, which can be seen, for example, in Fig. 1c at 8.5 ns and shortly after the reference and target returns. In standard MWI, these spurious reflections are a significant systematic error, because the measured range is effectively a weighted average of all returns. (Either polarization multiplexing or physically separate beam paths are required for the target and reference in MWI.) Second, there are no assumptions about the particular pulse shape. Third, effects due to dispersion are apparent as deviations in the spectral phase, $\varphi(\nu)$, from a linear slope. Fourth, strong self-consistency checks are possible through comparisons of the time-of-flight measurements centred at different carrier frequencies (by tuning the optical bandpass filter) and of the averaged time-of-flight and interferometric range measurements.

Rapid time-of-flight distance measurements of a moving target. Rapid update rates are important in applications such as formation flying or large-scale manufacturing, where the range information is used within a feedback system to orient the components. In our current configuration, it takes 200 μs to scan the entire 1.5-m ambiguity range, and therefore it is possible to capture the motion of a moving target, as is shown in Fig. 3, where sequential 200-μs traces are placed side by side to map the position of a moving target. A Hilbert transform is used to show only the magnitude squared (intensity) of the detected signal. From the time-of-flight, the absolute distance between the reference and target can be determined to within 3 μm for each trace (see Fig. 5 later). Note the dropout of information at ~1.6 s due to misalignment of the moving cart; for a standard c.w. interferometer with a range ambiguity of one wavelength, such a dropout would ruin the measurement, but here the system easily reacquires the absolute range. An object that moves out of the ambiguity range could be tracked with a simple unwrapping algorithm that should allow one to track an object moving as fast as 3,700 m s^{-1}.
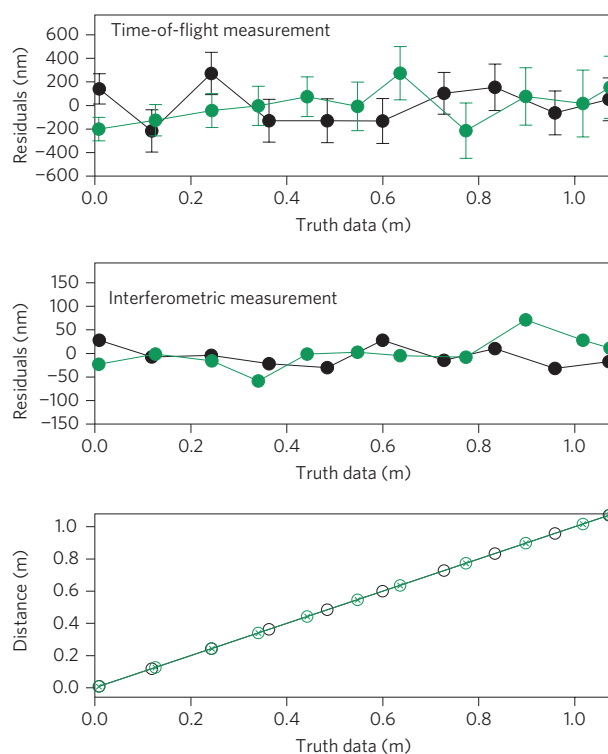
Figure 4 | Residuals of the measured time-of-flight and interferometric range measurements versus truth data from a commercial c.w. interferometer. The averaging period is 60 ms. Error bars are the standard deviation of the mean over the 60-ms period. Data taken with the fibre spool delay line are shown in black, and data without the spool are shown in green; as seen, the addition of the fibre delay has a negligible effect on the measurement. Although the interferometric data are much quieter, they become meaningful only when combined with the time-of-flight data to resolve the 780-nm range ambiguity.

High-precision absolute distance measurements using both time-of-flight and interferometric range measurements. For slowly moving targets, we can average down the time-of-flight measurement sufficiently to hand over to the more precise interferometric range measurement, as described after equation (1). We conducted a series of experiments to demonstrate this capability by comparing the results to 'truth' data supplied by a standard fringe counting interferometric distance meter[13]. In the first experiment, we recorded the reference-to-target distance at discrete steps over a ~1 m track. In satellite-to-satellite positioning the measurement could be at a range of a kilometre or longer. We therefore conducted two additional experiments with a fibre spool to extend the measurement range. Unfortunately, unlike space, optical fibre is nonlinear, dispersive, birefringent and backscatters the incident light. To counter nonlinearities, we simply chirped the outgoing signal pulse (necessary in any case for chirped-pulse amplification). To counter the dispersive effects, we included ~700 m of higher-dispersion fibre at the output of the LO laser but within the phase-locked loop, so that the effective delay on the two comb outputs remained, but their relative dispersion was approximately equal at the detector. The most important remaining effect was Rayleigh backscatter from the outgoing pulse, because it cannot be time-gated from the signal. In one experiment, we avoided this problem by using two identical ~1.14-km spools—one for the outgoing and one for the return signal—and measured the reference-to-target distance at the end of the 1.14-km fibre delay. These data mimic those needed to make remote measurements of
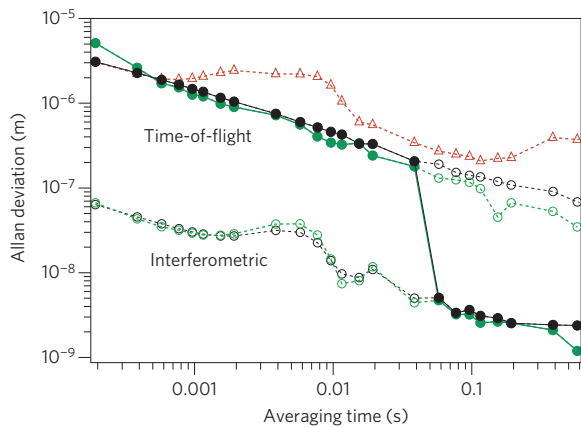
Figure 5 | Precision (Allan deviation) of the distance measurement versus averaging time. Three different measurements are shown: (i) an ~1 m reference-to-target distance without any fibre delay (black circles), (ii) an ~1 m reference-to-target distance with a 1.14-km fibre delay (green circles) and (iii) an ~1.14 km distance across a bidirectional fibre spool (red triangles). The Allan deviation is evaluated over a 5-s data run that is composed of a series of individual data points at the 200 μs update rate. For both reference-to-target distance measurements (with and without the fibre delay), both the time-of-flight and interferometric measurements are given. Solid circles show the experimental precision, which experiences a significant jump around 60 ms when the time-of-flight measurement is sufficiently stable compared to $\lambda_c/4$ and can be combined with the interferometric measurement. At shorter averaging times the interferometric data are still available, but provide only relative position information. For the 1.14-km distance measurement across the bidirectional fibre spool (red triangles), the precision of the time-of-flight distance is scaled to the group velocity of air. In this case, the uncertainty is dominated by actual length changes in the fibre and a 300-nm flicker floor from Rayleigh backscatter.

the pointing of a satellite, or the angle of a machined surface, through trilateration.

As shown in Fig. 4, we found no difference in system performance for the reference-to-target distance measurements with and without the 1.14-km fibre delay. For both our data and the truth data, the range was calculated for identical atmospheric conditions (air temperature, pressure and humidity) so that they shared a common ~1×10^{-7} uncertainty from variations in the atmospheric conditions[13]. An independently measured 1-μm drift in the air path (due to temperature change) was subtracted out of the data. At 60 ms averaging, the statistical error on the time-of-flight measurement was below 200 nm, with a systematic error evaluated at less than 100 nm. Because this uncertainty is below $\pm\lambda_c/2$, the distance measurement could be handed over to the interferometric range measurement, which had only a 20–30 nm scatter versus the truth data, consistent with the dominant uncertainty calculated from the estimated ~0.1 °C temperature variations between the two air paths[43] (see Fig. 2).

Figure 5 shows the precision of both the time-of-flight and interferometric measurements versus averaging time. Both with and without the fibre delay, the precision of the time-of-flight distance is $\sigma_{tof} = 3\ \mu m\ (T_{update}/T)^{1/2}$, where T is the averaging period. This scatter is about twice that expected from the measured white noise on the signal and results from ~20 fs residual timing jitter between the combs. The precision of the interferometric distance is roughly $\sigma_{int} = 100\ nm\ (T_{update}/T)^{1/2}$, reaching 5 nm at 60 ms and continuing to drop below 3 nm at 0.5 s. It is limited by the residual carrier phase jitter between the combs. For both range measurements, tighter phase-locking or post-correction of the data from monitoring of the error signals will improve the precision[40,44,45].

Finally, in a third experiment, we replaced the dual fibre spools with a single, bidirectional spool and measured the delay between a reference reflection before the 1.14-km fibre spool and the target. The relative uncertainty, also shown in Fig. 5, is limited by Rayleigh backscattering, which gave rise to a 'flicker' noise floor of ~300 nm, which was too large to permit a confident 'handover' to the interferometric range measurement. At longer times, the uncertainty increases due to actual ~1 μm s^{-1} fibre length changes from temperature effects.

The comb repetition rate of $T_r^{-1} \approx 100$ MHz sets the ambiguity range of our system to $R_A = T_r v_{group}/2 = 1.5$ m, adequate for most practical situations, but clearly lower than the fibre delay, equivalent to 1.8 km of air. To remove this ambiguity, we switched the roles of the signal and LO lasers and used the Vernier effect. Because of the difference in repetition rates, a distance measured normally and a second distance measured with the lasers switched differs by $m\Delta R_A$, where $\Delta R_A = \Delta T_r v_{group}/2$ is the difference in ambiguity ranges, and m is an integer giving the number of ambiguity ranges by which the true distance exceeds R_A. Therefore, with the two measurements, we can find m and resolve any ambiguity up to the now larger ambiguity range of $v_{group}/(2\Delta f_r) = 30$ km, where $\Delta f_r = (T_{update})^{-1} \approx 5$ kHz is the difference in comb repetition rates. Applying this technique to the fibre spool we measured a fibre length of 1,139.2 m, in good agreement with a standard optical time-domain reflectometry measurement (using the same group index) of $1,138.4 \pm 1$ m.

The limit to the fractional accuracy in the time-of-flight and interferometric range measurements is ultimately the fractional accuracy in the rf timebase and optical frequency, respectively. Here, we rely on an rf time base (hydrogen maser) that can support better than 1×10^{-13} fractional ranging resolution, that is, 3 nm in 30 km or below the systematic uncertainty. The fractional accuracy of the carrier frequency will depend on the underlying c.w. reference laser, which can be stabilized to a calibrated reference cavity, a molecular reference, or a self-referenced frequency comb[46,47]. (Here, we stabilized the carrier frequency to a reference cavity with ~30 kHz wander and monitored the exact frequency with a self-referenced frequency comb.) The fractional accuracy provided by a reference cavity or molecular reference is sufficient for nanometre-scale measurements at short ranges, or for differential range measurements at long ranges. Nanometre-scale absolute ranging at long distances would require a fully self-referenced comb[46], with its significant added technical complexity. Of course, for extreme precision at very long ranges, the entire system could be based on an optical clock[47], providing an increase of greater than 1×10^4 in accuracy, with effectively unlimited operation distances.

Discussion

The data above illustrate the ability of this system to measure the range between multiple reflections over a large range window (ambiguity range) at a short update rate and at long ranges. Equally important are the built-in checks on hidden systematics by comparing time-of-flight and interferometric range measurements. Although the detection and processing is straightforward, the clear technical challenge lies in the dual, coherent frequency comb sources, particularly for satellite applications. Optical frequency combs have been proposed previously for future space missions using optical clocks, but current combs remain mainly laboratory instruments, albeit with continued progress in environmentally robust fibre-based combs[46,48,49]. Fortunately, the comb source requirements here are simpler in two regards than those for the fully self-referenced octave-spanning combs needed to support current optical clocks. First, although the combs are phase-locked to hertz-level linewidths here, the absolute linewidth actually need only be below Δf_r to cover the full 1.5-m ambiguity range.

(Narrower linewidths are required only for extremely long-range operation beyond $v_{group}/\Delta f_r \approx 30$ km.) Second, the comb output need only span ~10–20 nm optical bandwidth rather than a full octave. Nevertheless, significant engineering will be required to space-qualify such a system. We do note that the basic technique is not limited to fibre-based mode-locked lasers, and other passively mode-locked lasers[50] may provide a route to a more robust and compact system.

As stated earlier, for either large-scale manufacturing or formation flying, it is often the angle or pointing of a target object that is most critical[12]. The pitch and yaw of the object can be determined through trilateration, where the angle is calculated from the distance to several reference points spanning the target. Our approach is well suited to carrying out this measurement, because the time gating of multiple reflections allows one to collect and process data for all trilateration reference points on the same photodiode and digitizer, saving both space and power. The wide ambiguity range and high update rate can support rapid reconfiguration of the target objects.

For active stabilization of absolute distances, or pointing angles, it would be beneficial to improve the time-of-flight measurement to below $\lambda_c/4$ in a single scan so that interferometric precision could be reached in a single update time, T_{update}. The time-of-flight measurement uncertainty will improve by increasing the signal pulse bandwidth up to the available ~4 THz source bandwidth (assuming a corresponding reduction in the residual comb jitter). However, the pulse bandwidth BW is constrained by the relationship $BW < T_{update}/2T_r^2$ (to achieve adequate sampling), so a larger bandwidth implies a lower update rate. This constraint can be removed by coherently combining multiple detection channels at different wavelength bands across the source. With this approach, nanometre-level precision should be possible at less than a millisecond update rate.

In conclusion, frequency comb based LIDAR offers a host of powerful features—precision, stability, speed, large-range ambiguity, low light level operation, multiplexing capabilities, flexibility and spurious reflection immunity—that, as a whole, are unavailable in existing approaches.

Methods

The linear optical sampling scheme presented here is relatively straightforward, but contains a few technical subtleties. In our linear optical sampling picture, signal and LO pulses arrive at the detector at a rate of ~100 MHz and with varying delays between them. The signal and LO pulse overlap is integrated over the detector response time (~1/100 MHz) to yield a single voltage, which is then synchronously digitized with the LO repetition rate. Sampling is done with a 110 MHz balanced detector that allows us to suppress amplitude noise in the relatively high power LO. To eliminate detector ringing effects, the signal is low-pass filtered at 50 MHz (which also eliminates any nonsensical signal above the Nyquist frequency set by the LO sampling rate). Once the signal and LO are combined on the same detector, the measurement is insensitive to electronic phase shifts as long as the system remains linear. Saturation of detectors and amplifiers is carefully avoided.

For time-of-flight distance measurements with resolution smaller than 200 nm, a few pitfalls arise. In virtual time, the LO samples the signal laser $T_r/\Delta T_r = 19,260$ times per signal repetition period, T_r. This gives an effective sample step size of 78 μm. For ease in processing one might be tempted to set up the system so that after every 19,260 samples the signal and the LO have the same phase. However, systematics related to the pulse shape limit our ability to measure the centre of our peaks below a precision of 300 nm with a 78-μm step size. Instead we arrange our phase locks so that the pulses overlap every $19,260 \times 51$ samples. Averaging sequential frames then allows us to effectively subdivide the 78-μm step size by 51, which is sufficient to achieve sub-100-nm resolution. It was also found that the use of interleaved ADCs (analog-to-digital converters) in the digitizer can lead to 100-nm-level scatter in the data. Fortunately, 100 MHz single ADC digitizers are now widely available.

For the interferometric measurement, we must account for the phase factor ψ, defined in the text as $\psi = \pi + \varphi_{Gouy}$. The factor π arises from the reflection from the air–glass interface at the target. The reference pulse occurs from a glass–air interface and suffers no such phase shift. The Gouy phase shift is dependent on the actual distance and we use a separate measurement of the beam Rayleigh range to calculate this phase shift from the time-of-flight distance data.

In our experiment, the processing is not real time. Rather, we collect the raw data and post-process it on a PC. The processing is done on a 'scan-by-scan' basis. The 19,260 data points from each ~200-μs-long scan are first high-pass-filtered at 5 MHz and then searched for the three largest peaks, the first two of which are from the front and back surfaces of the reference flat and the last one from the target. Two copies of the data are then generated: one with a 60-ps time window (the exact width is not important) around the appropriate reference reflection and one with a 60-ps time window about the target reflection. The 19,260 data points are then truncated to a length that has only low numbers in its prime factorization (for example, 19,200) and fast Fourier transformed (FFT). The spectral phase is extracted from the FFT and fit across ~0.4 THz of bandwidth to equation (1) and further processed as described in the text. The most computationally intensive operation is the FFT, and real-time processing of the data should be possible with modern field programmable gate arrays.

References

1. Cash, W., Shipley, A., Osterman, S. & Joy, M. Laboratory detection of X-ray fringes with a grazing-incidence interferometer. *Nature* **407,** 160–162 (2000).
2. White, N. X-ray astronomy—Imaging black holes. *Nature* **407,** 146–147 (2000).
3. Gendreau, K. C., Cash, W. C., Shipley, A. F. & White, N. MAXIM Pathfinder X-ray interferometry mission. *Proc. SPIE—Int. Soc. Opt. Eng.* **4851,** 353–364 (2003).
4. ESA. XEUS: X-ray evolving-universe spectroscopy. *ESA CDF Study Report* **CDF-31(A),** 1–237 (2004).
5. Fridlund, M. Future space missions to search for terrestrial planets. *Space Sci. Rev.* **135,** 355–369 (2008).
6. Fridlund, C. V. M. Darwin-the infrared space interferometry mission. *ESA Bulletin* **103,** <http://www.esa.int/esapub/bulletin/bullet103/fridlund103.pdf> 20–25 (2000).
7. Lawson, P. R. & Dooley, J. A. Technology plan for the terrestrial planet finder interferometer. *Publ. Jet Propulsion Laboratory* **05–5,** 1–149 (2005).
8. Coroller, H. L., Dejonghe, J., Arpesella, C., Vernet, D. & Labeyrie, A. Tests with a Carlina-type hypertelescope prototype. *Astron. Astrophys.* **426,** 721–728 (2004).
9. Lemmerman, L. *et al.* Earth science vision: platform technology challenges. Scanning the present and resolving the future. *Proc. IEEE 2001 International Geoscience and Remote Sensing Symposium* (2001).
10. Turyshev, S. G. & Shao, M. Laser astrometric test of relativity: Science, technology and mission design. *Int. J. Mod. Phys. D* **16,** 2191–2203 (2007).
11. Turyshev, S. G., Lane, B., Shao, M. & Girerd, A. A search for new physics with the BEACON mission. Preprint at <http://arxiv:0805.4033v1> (2008).
12. Estler, W. T., Edmundson, K. L., Peggs, G. N. & Parker, D. H. Large-scale metrology—an update. *CIRP Ann. Manuf. Technol.* **51,** 587–609 (2002).
13. Bobroff, N. Recent advances in displacement measuring interferometry. *Meas. Sci. Technol.* **4,** 907–926 (1993).
14. Nagano, S. *et al.* Displacement measuring technique for satellite-to-satellite laser interferometer to determine Earth's gravity field. *Meas. Sci. Technol.* **15,** 2406–2411 (2004).
15. Pierce, R., Leitch, J., Stephens, M., Bender, P. & Nerem, R. Inter-satellite range monitoring using optical inteferometry. *Appl. Opt.* **47,** 5007–5019 (2008).
16. Beck, S. M. *et al.* Synthetic aperture imaging LADAR: laboratory demonstration and signal processing. *Appl. Opt.* **44,** 7621–7629 (2005).
17. Lucke, R. L., Richard, L. J., Bashkansky, M., Reintjes, J. & Funk, E. E. Synthetic aperture ladar. *Naval Research Laboratory*, FR 7218–02-10,051 1–28 (2002).
18. Minoshima, K. & Matsumoto, H. High-accuracy measurement of 240-m distance in an optical tunnel by use of a compact femtosecond laser. *Appl. Opt.* **39,** 5512–5517 (2000).
19. Dandliker, R., Thalmann, R. & Prongue, D. Two-wavelength laser interferometry using superheterodyne detection. *Opt. Lett.* **13,** 339–341 (1988).
20. Williams, C. C. & Wickramasinghe, H. K. Absolute optical ranging with 200-nm resolution. *Opt. Lett.* **14,** 542–544 (1989).
21. Stone, J. A., Stejskal, A. & Howard, L. Absolute interferometry with a 670-nm external cavity diode laser. *Appl. Opt.* **38,** 5981–5994 (1999).
22. Yang, H. J., Deibel, J., Nyberg, S. & Riles, K. High-precision absolute distance and vibration measurement with frequency scanned interferometry. *Appl. Opt.* **44,** 3937–3944 (2005).
23. Schuhler, N., Salvade, Y., Leveque, S., Dandliker, R. & Holzwarth, R. Frequency-comb-referenced two-wavelength source for absolute distance measurement. *Opt. Lett.* **31,** 3101–3103 (2006).
24. Salvade, Y., Schuhler, N., Leveque, S. & Le Floch, S. High-accuracy absolute distance measurement using frequency comb referenced multiwavelength source. *Appl. Opt.* **47,** 2715–2720 (2008).
25. Jin, J., Kim, Y.-J., Kim, Y. & Kim, S.-W. Absolute length calibration of gauge blocks using optical comb of a femtosecond pulse laser. *Opt. Express* **14,** 5968–5974 (2006).
26. Fox, R. W., Washburn, B. R., Newbury, N. R. & Hollberg, L. Wavelength references for interferometry in air. *Appl. Opt.* **44,** 7793–7801 (2005).

27. Lay, O. P. *et al.* MSTAR: a submicrometer, absolute metrology system. *Opt. Lett.* **28,** 890–892 (2003).

28. Hänsch, T. W. Nobel Lecture: Passion for precision. *Rev. Mod. Phys.* **78,** 1297–1309 (2006).

29. Hall, J. L. Nobel Lecture: Defining and measuring optical frequencies. *Rev. Mod. Phys.* **78,** 1279–1295 (2006).

30. Ye, J. Absolute measurement of long, arbitrary distance to less than an optical fringe. *Opt. Lett.* **29,** 1153–1155 (2004).

31. Joo, K.-N. & Kim, S.-W. Absolute distance measurement by dispersive interferometry using a femotsecond pulse laser. *Opt. Express* **14,** 5954–5960 (2006).

32. Swann, W. C. & Newbury, N. R. Frequency-resolved coherent lidar using a femtosecond fiber laser. *Opt. Lett.* **31,** 826–828 (2006).

33. Joo, K. N., Kim, Y. & Kim, S. W. Distance measurements by combined method based on a femtosecond pulse laser. *Opt. Express* **16,** 19799–19806 (2008).

34. Newbury, N. R., Swann, W. C. & Coddington, I. Lidar with femtosecond fiber-laser frequency combs. *14th Coherent Laser Radar Conference* (Snowmass, Colorado, 2007).

35. Keilmann, F., Gohle, C. & Holzwarth, R. Time-domain and mid-infrared frequency-comb spectrometer. *Opt. Lett.* **29,** 1542–1544 (2004).

36. Schiller, S. Spectrometry with frequency combs. *Opt. Lett.* **27,** 766–768 (2002).

37. Yasui, T., Kabetani, Y., Saneyoshi, E., Yokoyama, S. & Araki, T. Terahertz frequency comb by multifrequency-heterodyning photoconductive detection for high-accuracy, high-resolution terahertz spectroscopy. *Appl. Phys. Lett.* **88,** 241104 (2006).

38. Coddington, I., Swann, W. C. & Newbury, N. R. Coherent multiheterodyne spectroscopy using stabilized optical frequency combs. *Phys. Rev. Lett.* **100,** 013902 (2008).

39. Schlatter, A., Zeller, S. C., Pashcotta, R. & Keller, U. Simultaneous measurement of the phase noise on all optical modes of a mode-locked laser. *Appl. Phys. B* **88,** 385–391 (2007).

40. Giaccari, P., Deschenes, J.-D., Saucier, P., Genest, J. & Tremblay, P. Active Fourier-transform spectroscopy combining the direct RF beating of two fiber-based mode-locked lasers with a novel referencing method. *Opt. Express* **16,** 4347–4365 (2008).

41. Dorrer, C., Kilper, D. C., Stuart, H. R., Raybon, G. & Raymer, M. G. Linear optical sampling. *IEEE Photon. Technol. Lett.* **15,** 1746–1748 (2003).

42. Dorrer, C. High-speed measurements for optical telecommunication systems. *IEEE J. Quantum Electron.* **12,** 843–858 (2006).

43. Ciddor, P. E. & Hill, R. J. Refractive index of air. 2. Group index. *Appl. Opt.* **38,** 1663–1667 (1999).

44. Telle, H. R., Lipphardt, B. & Stenger, J. Kerr-lens, mode-locked lasers as transfer oscillators for optical frequency measurements. *Appl. Phys. B* **74,** 1–6 (2002).

45. Stenger, J., Schnatz, H., Tamm, C. & Telle, H. R. Ultraprecise measurement of optical frequency ratios. *Phys. Rev. Lett.* **88,** 073601 (2002).

46. Newbury, N. R. & Swann, W. C. Low-noise fiber laser frequency combs. *J. Opt. Soc. Am. B* **24,** 1756–1770 (2007).

47. Rosenband, T. *et al.* Frequency ratio of Al$^+$ and Hg$^+$ single-ion optical clocks; metrology at the 17th decimal place. *Science* **319,** 1808–1812 (2008).

48. Hartl, I., Imshev, G., Fermann, M. E., Langrock, C. & Fejer, M. M. Integrated self-referenced frequency-comb laser based on a combination of fiber and waveguide technology. *Opt. Express* **13,** 6490–6496 (2005).

49. Baumann, E. *et al.* A high-performance, vibration-immune fiber-laser frequency comb. *Opt. Lett.* **34,** 638–640 (2009).

50. Koch, B. R., Fang, A. W., Cohen, O. & Bowers, J. E. Mode-locked silicon evanescent lasers. *Opt. Express* **15,** 11225–11233 (2007).

Author contributions

I.C., W.C.S. and N.R.N. contributed equally to this work. L.N. assisted with the data analysis.

Additional information

Reprints and permission information is available online at http://npg.nature.com/reprintsandpermissions/. Correspondence and requests for materials should be addressed to I.C. and N.R.N.